Eur. Phys. J. D **38**, 85–91 (2006)
DOI: 10.1140/epjd/e2006-00013-7

THE EUROPEAN PHYSICAL JOURNAL D

Steric effect in O^+/H_2 and H^+/H_2O collisions

Charge transfer in H_2O^+ and H_3O^+ collision intermediate systems

M. Kimura[1], L. Pichl[2,a], Y. Li[3], H.-P. Liebermann[3], R.J. Buenker[3], and I.F. Schneider[4]

[1] Graduate School of Sciences, Kyushu University, Fukuoka 812-8581, Japan
[2] Max Planck Institute for the Physics of Complex Systems, Nöthnitzer Str. 38, 01187 Dresden, Germany
[3] Fachbereich C-Mathematik und Naturwissenschaften, Bergische Universität Wuppertal, 42119 Wuppertal, Germany
[4] UFR Sciences et Techniques, Université du Havre, 25 rue Philippe Lebon, B.P. 540, 76058 Le Havre Cedex, France

Received 2nd August 2005 / Received in final form 2nd December 2005
Published online 17 January 2006

Abstract. The positive water and hydronium ions are of interest in a variety of chemical and biological applications. Here we study the steric effect in charge transfer collisions, i.e. the spatial dependence of single electron capture, in collisions mediated by these ions. In particular, the steric effect is demonstrated in the $O^+(^2D)/H_2$ and H^+/H_2O charge transfer collisions in the energy range of 100 eV/amu to 10 keV/amu.

PACS. 34.70.+e Charge transfer – 34.50.Gb Electronic excitation and ionization of molecules; intermediate molecular states (including lifetimes, state mixing, etc.) – 31.15.Ar Ab initio calculations

1 Introduction

In the charge-transfer collisions of atomic ions with molecules, the relative orientation of target and projectile as well as the details of potential energy surfaces are known to have a limited effect on the integral cross-sections, at least in the keV/amu energy range (collision velocity 0.2 a.u. and above). Nevertheless, a considerable steric effect may be present even at those high energies when the differential cross-sections or transition probabilities along particular collision trajectories are studied. These phenomena have been somewhat neglected in the past, due to both the experimental difficulties in orienting neutral molecular targets and the theoretical complexity inherent in polyatomic collisional systems, which typically involves rovibrational motion of the colliding system in a number of coupled electronic states. Here, we would like to look at these effects more closely.

Owing to large collision velocities in the keV/amu energy range, the period of (ro)vibrational motion of the target molecule is much larger than the collision time, and hence the nuclear geometry of the target can be kept fixed. In addition, the presence of long-range Coulomb interaction in ion-ion channels may dominate the details of local electronic structures, imposing thus a partial spherical symmetry on the system. That is often the reason why the integral charge transfer cross-sections can be well estimated by using a few, if not a single one, orientations of the collisional molecular ion system. Much theoretical work has been devoted to the development and accuracy assessment of such approximations [1,2].

However, the electron capture process may depend on the orientation of the projectile and details of the potential energy surface if either the collision trajectory or target orientation is resolved. It is the purpose of this paper to demonstrate the steric effect in the H_2O^+ and H_3O^+ systems. To that aim, we first study a central collision of $O^+(^2D)$ with H_2 molecule, depending on the angle between projectile velocity and molecular axis. Next we proceed to the collision of H^+ with H_2O using a proton beam oriented perpendicularly to the plane of the water molecule, and screen the asymptotic electron capture probabilities along a two-dimensional set of impact parameter vectors.

The paper is organized as follows. In Section 2, the ab initio calculations and the electronic state close-coupling formalism are summarized along with references to previous work [3,4]. Section 3 explains the steric effect on electron capture probabilities and cross-sections for the H_2O^+ and H_3O^+ collision intermediates, and discusses the accuracy of the integral charge transfer cross-sections obtained with the central collision approximation. Concluding remarks close the paper in Section 4. Atomic units are used throughout the paper.

2 Theoretical model

The potential energy curves (PEC) for H_2O^+ and H_3O^+ systems were obtained ab initio for the most general

[a] e-mail: lukas@pichl.jp
On summer leave from: International Christian University, Osawa 3-10-2, Mitaka, Tokyo 181-8585, Japan.

Table 1. Convergence of the ground-state energy (in Hartree) for H_2O^+ and H_3O^+ ions with respect to the selection threshold τ (in micro-Hartree) and the basis set cc-pvNz for $N = T, Q$. Results both for the equilibrium geometry (R_{eq}) and the asymptotic separation of target and projectile ($R_{as} = 10$ a.u.) are shown.

	N	τ	$E(2\tau)$	$E(\tau)$	E_{extrap}	Full CI	%	SAFs
					H_2O^+			
R_{eq}	T	0.0	–75.861718	–75.861718	–75.861718	–75.878983	93.3	36882
	T	0.2	–75.860029	–75.860993	–75.861567	–75.878757	93.3	27991
	T	0.6	–75.855713	–75.859042	–75.861392	–75.878499	93.3	22065
	T	2.0	–75.841073	–75.850913	–75.861027	–75.877889	93.4	13811
	T	8.0	–75.802505	–75.825186	–75.860027	–75.876289	93.6	5876
	Q	0.0	–75.878418	–75.878418	–75.878418	–75.896176	93.4	81415
	Q	0.2	–75.874794	–75.876779	–75.878282	–75.895990	93.4	47560
	Q	0.6	–75.866559	–75.872678	–75.878172	–75.895841	93.4	33340
	Q	2.0	–75.844062	–75.858934	–75.878045	–75.895613	93.4	17642
	Q	8.0	–75.800797	–75.823307	–75.876596	–75.893763	93.5	5818
R_{as}	T	0.0	–75.655537	–75.655537	–75.655537	–75.661931	95.9	70673
	T	0.2	–75.654766	–75.655003	–75.655306	–75.661645	95.9	5399
	T	0.6	–75.653898	–75.654510	–75.655285	–75.661602	95.9	4240
	T	2.0	–75.650904	–75.653033	–75.655120	–75.661362	96.0	3103
	T	8.0	–75.642157	–75.647229	–75.655082	–75.661099	96.1	1756
	Q	0.0	–75.667911	–75.667911	–75.667911	–75.674584	95.9	154602
	Q	0.2	–75.666950	–75.667240	–75.667601	–75.674205	95.9	7535
	Q	0.6	–75.665911	–75.666614	–75.667563	–75.674147	96.0	5836
	Q	2.0	–75.662483	–75.664658	–75.667524	–75.674054	96.0	4126
	Q	8.0	–75.649828	–75.657101	–75.667360	–75.673704	96.1	2240
					H_3O^+			
R_{eq}	Q	0.0	–76.609942	–76.609942	–76.609942	–76.623875	94.9	64447
	Q	0.2	–76.606110	–76.607802	–76.609033	–76.622687	94.9	38256
	Q	0.6	–76.599276	–76.604368	–76.608924	–76.622520	95.0	27726
	Q	2.0	–76.579319	–76.592836	–76.608837	–76.622203	95.1	16206
	Q	8.0	–76.529676	–76.558059	–76.608364	–76.620848	95.4	6385
R_{as}	Q	0.0	–76.350540	–76.350540	–76.350540	–76.366162	94.3	64447
	Q	0.2	–76.347035	–76.348336	–76.349293	–76.364432	94.5	32500
	Q	0.6	–76.341753	–76.345730	–76.349205	–76.364292	94.5	24524
	Q	2.0	–76.324910	–76.336595	–76.349050	–76.363930	94.6	15391
	Q	8.0	–76.278016	–76.305904	–76.348731	–76.362801	94.9	6618

molecular symmetries by using the multireference single- and double-excitation configuration interaction (MRD-CI) method [5–8].

A Gaussian ($6s3p2d1f$) basis contracted to [$4s3p2d1f$] was used for the hydrogen atom, while a ($12s6p3d2f$) basis set contracted to [$5s4p3d2f$] was employed for the oxygen atom. All basis sets used for the scattering are of the cc-pVQZ type [9]. In addition, a diffuse [$2s2p2d$] basis centered at oxygen atom is employed to describe the Rydberg electronic states of the water molecule. The convergence with respect to the basis set and other ab initio parameters is discussed below.

The selection threshold and the number of configurations are 2.0×10^{-7} a.u. and 500,000 for H_2O^+, and 8.0×10^{-7} a.u. and 200,000 for H_3O^+, respectively. The effect of all unselected configurations is checked by using the perturbative energy extrapolation procedure [8]. The resulting highly correlated wavefunctions are used to obtain the nonadiabatic coupling matrix elements by a numerical differentiation method [10]. The origin of electronic coordinates is placed at the molecular center of mass for all geometries.

In the case of H_2O^+, the internuclear distance of hydrogen atoms was fixed at 1.4 and 1.6 to estimate the effect of hydrogen molecular vibrations. The potential energy surfaces for the doublet states (asymptotically corresponding to the metastable $O^+(^2D,^2P)$ ions were projected along three O^+ lines passing through the center of the H–H line at the angles $\gamma = 0$, $\pi/4$ and $\pi/2$.

In the case of H_3O^+, the target water molecule is fixed at the equilibrium geometry. The trajectories of the impacting proton are perpendicular to the plane of the water molecule $[x, y]$, which they intersect at: (1) the oxygen atom (z-direction approach), (2) on the OS line, where S is the center of H–H line, or (3) the OP line, where OP and OS are perpendicular in-plane lines. The nuclear geometry is invariant with respect to an inversion along the OS line. Potential energy curves and nonadiabatic couplings were obtained for three magnitudes of the impact parameter relative to the oxygen atom, $b = 0.9$, 1.8, and 3.6. The geometry of the collision is shown in Figure 1.

Table 1 shows the ground-state energies for the H_2O^+ and H_3O^+ ions, and the asymptotic energies of the target and projectile (H_2 with O^+, and H_2O with H^+,

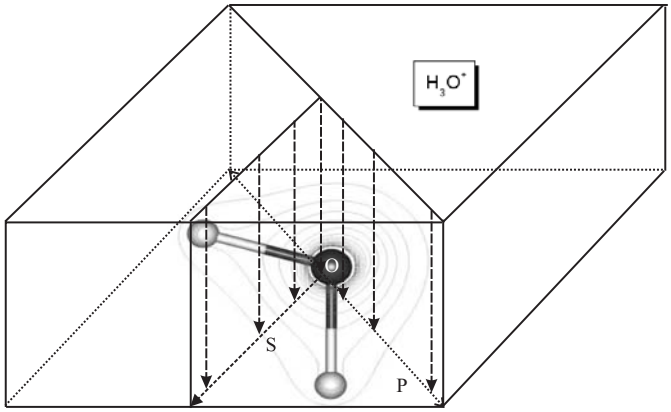

Fig. 1. Collision of H^+ with H_2O: beam of trajectories perpendicular to the water molecule plane. The beam intersects with the plane along two lines: (1) O–S line, where S is located in the middle of H–H line ($\phi = 0$), and (2) O–P line ($\phi = \pi/2$), perpendicular to O–S. Four values of impact parameters, 0.9, 1.8 and 3.6 a.u. are considered, resulting in 10 straight-line trajectory rays.

Table 2. Asymptotic energies (in Hartree) for H_2O^+ and H_3O^+ fragments. The cc-pvNZ basis set is used with either N = T or N = Q. Data both for single (S), and single and double (SD) excitation CI are shown.

	CI	N	E_{extrap}	FCI	SAFs
O^+	SD	T	–74.485870	–74.489034	6519
	SD	Q	–74.497511	–74.500855	25372
	S	T	–74.393436	–74.393701	131
	S	Q	–74.398406	–74.398678	253
O	SD	T	–74.974990	–74.981533	9814
	SD	Q	–74.989796	–74.996725	38101
	S	T	–74.827703	–74.827897	151
	S	Q	–74.832140	–74.832339	293
H_2	SD	T	–1.172753	–1.173469	471
	SD	Q	–1.173839	–1.174566	821
	S	T	–1.133062	–1.133062	26
	S	Q	–1.133469	–1.133469	32
H_2O	SD	T	–76.324450	–76.339437	21178
	SD	Q	–76.342915	–76.358633	47132
	S	T	–76.061257	–76.061257	128
	S	Q	–76.066204	–76.066204	190

respectively) separated by the distance $R = 10$ a.u. The distance is measured from the center of the H_2 molecule in the former case, and from the oxygen atom in the latter case. The convergence of MRD-CI results is shown in Table 1 with respect to the basis set (cc-pvTZ and cc-pvQZ), configuration selection threshold τ and number of configurations. The percentage of reference configurations shown in Table 1 (c2 criterion) also demonstrates the degree of convergence with respected to the selected configurations.

Energy values from the CI calculations are extrapolated as a function of the selection threshold τ. The extrapolation is explicitly based on the 2nd order perturbation theory and Davidson correction, instead of using triple and higher-order excitations. Let us note that the accuracy of this approach has been previously tested and proved in our benchmark papers on MRD-CI vs. full CI for systems with number of electrons corresponding to present H_2O^+ and H_3O^+ molecular ions [11,12]. The ground-state energies for O^+, O, H_2 and H_2O fragments are added in Table 2. These data illustrate that inclusion of double excitations lowers the ground-state energy substantially more than the substitution of the cc-pvTZ basis set with the larger cc-pvQZ.

The collision dynamics at the keV/amu energy range is given by coupled equations [1,3] in the above basis of electronic-state amplitudes f_n on potential energy surfaces Γ labelled by the impact parameters b,

$$\left[i\frac{d}{dz} - \frac{E_n(R) - E_0}{v}\right] f_n^{\boldsymbol{b}}(z;\Gamma) = \sum_{n'}{}' c_{nn'} f_{n'}^{\boldsymbol{b}}(z;\Gamma). \quad (1)$$

Here v is the velocity, $z = vt$ is the coordinate along the projectile's trajectory, $R = (b^2 + z^2)^{1/2}$, $c_{nn'}$ is the coupling matrix and E_0 is the collision energy. The equations are solved for the initial condition $f_{n'}^{\boldsymbol{b}}(-\infty) = \delta_{nn'}$. The cross-section formula for electron capture in the general case is obtained by integration over the plane of impact parameters and averaging over the molecular orientations Γ as appropriate,

$$\sigma_{nn'} = \int \mathrm{d}b_x \mathrm{d}b_y \left\langle |f_{n'}^{\boldsymbol{b}}(\infty;\Gamma)|^2 \right\rangle_\Gamma . \quad (2)$$

Details of the above formulation for ion-atom collisions ($f^{\boldsymbol{b}} \to f^b$, single PEC Γ) can be found in references [1,13–16]; the ion-diatomic collision case is dealt with e.g. in references [2,17–19] (PEC are parameterized by one angle γ). In the present ion-triatomic case, H^+/H_2O collision, the molecular plane is aligned perpendicular to the proton beam, and hence each value of the impact parameter corresponds to its potential energy surface Γ. Introducing polar coordinates for the impact parameter vector, $\boldsymbol{b} \to (b, \phi)$, the cross-section formula then reads

$$\sigma_\perp = 2\int_0^\infty \mathrm{d}b \int_0^\pi \mathrm{d}\phi\, b\, p_{n'}(b,\phi;R(b,z\to\infty)), \quad (3)$$

where $p_{n'}(b,\phi;R(b,z\to\infty))$ is the transition probability given by $|f_{n'}^{(b,\phi)}(\infty;\perp)|^2$.

3 Steric effect in the electron capture

Based on the MRD-CI potential energy curves and couplings, we solved the coupled equations (1) along the collision trajectories and for target orientations defined in Section 2. The next two subsections discuss the steric effect seen in the resulting charge transfer probabilities.

3.1 Collision of $O^+(^2D)$ with H_2

Figure 2 (upper panel) displays the manifold of doublet H_2O^+ potential energy curves, which asymptotically correspond to $O^+(^2D,^2P)$ states, or O states in the electron capture channel. Excited states of H_2/H_2^+ are also

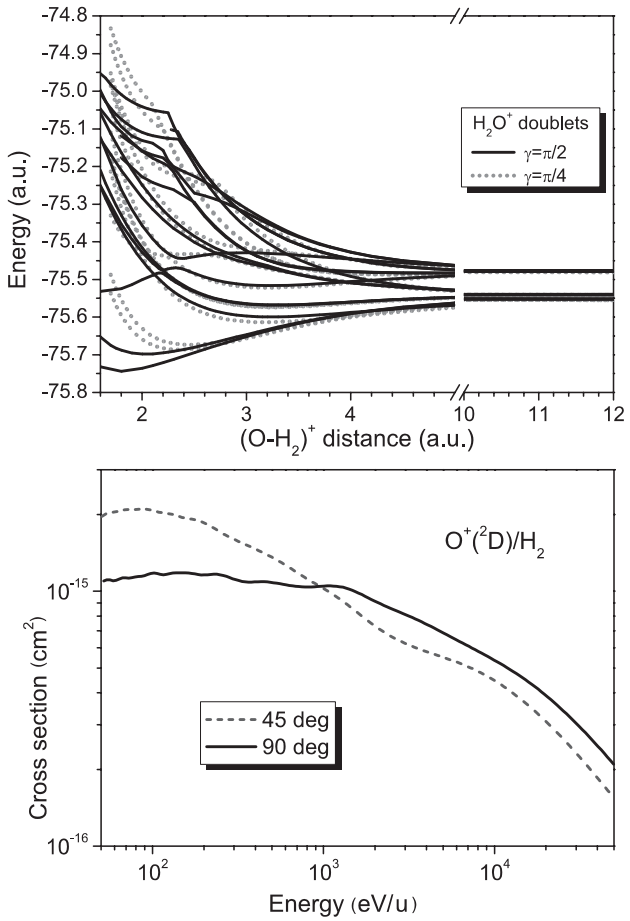

Fig. 2. Electron capture cross-section for collisions of $O^+(^2D)$ with the H_2 molecule using fixed-γ potential energy surfaces for $\gamma = \pi/2$ and $\gamma = \pi/4$.

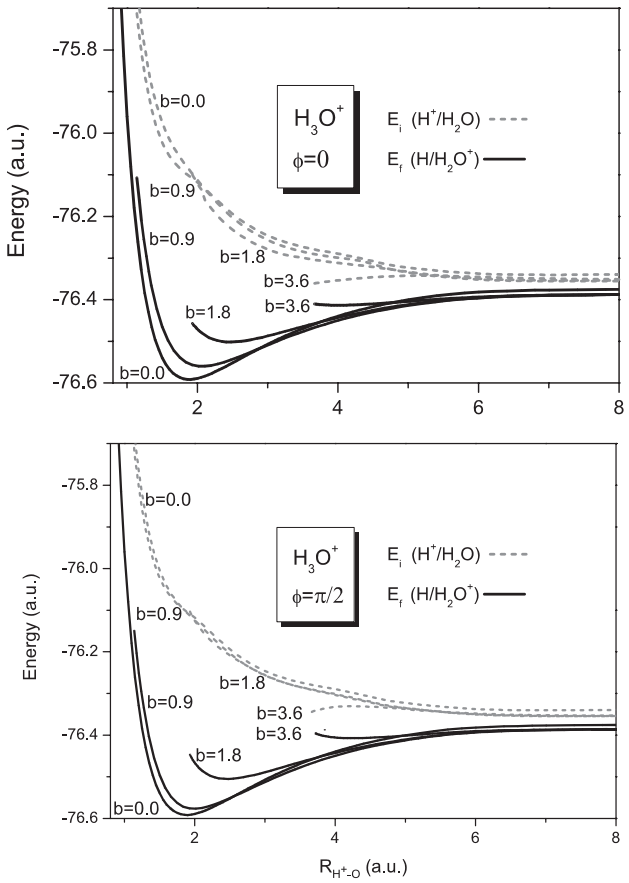

Fig. 3. Potential energy curves of the initial and final charge transfer state ($^1A_1$ symmetry) for $\phi = 0$ (upper panel) and $\phi = \pi/2$ (lower panel) for four impact parameter values ($R > b$).

included. The PEC passing through the target center are shown for two angles between $\gamma = \pi/4$ (dashed line, A' and A'' symmetry) and $\gamma = \pi/2$ (full line, A_1, A_2, B_1, B_2 symmetry). Although both groups of PEC are similar for $|HH| \sim 2.5$ (polarization interaction), substantial differences arise at lower collision distances. Owing in part to symmetry reasons, the PEC for $\gamma = \pi/4$ have higher energies than those for $\gamma = \pi/2$. The lower panel of Figure 2 shows the cross-section for electron capture from the $O^+(^2D)$ projectile in fixed γ approximation [4,17,18]. The steric effect can be clearly seen in Figure 2.

The relatively small difference between the physical cross-section and the cross-sections calculated on the potential energy surfaces with frozen γ allows us in principle to use the fixed γ potential energy surfaces for estimating the real cross-section value, for which the full manifold of γ would otherwise be required. For instance, the resulting error in the order of dozen % (cf. the difference of the two curves for $\gamma = \pi/4$ and $\gamma = \pi/2$ in Fig. 2) would still be smaller than the accuracy of experimental data for the same process. Or, since $\gamma = \pi/4$ is the middle value interpolating the extreme orientations $\gamma = \pi/2$ and $\gamma = 0$, the error resulting from using the potential energy surface with γ frozen at $\pi/4$ would only be about 30% of the total cross-section value for keV/amu energies. Data in the measurements of $O^+(^2D)$ [20–22] vary by a factor of 2 among experimental groups, which is more than what results from using the approximate potential energy surfaces with a frozen value of γ.

A detailed discussion of the integral cross-sections for electron capture on H_2 by $O^+(^2D, ^2P, ^4S)$ can be found in references [3,4] along with a comparison to recent measurements [23,24]. The reasons for experimental errors and applicability of the frozen potential energy surfaces to other systems are discussed below.

3.2 Collision of H^+ with H_2O

The potential energy curves for the proton beam intersecting the water molecular plane on the OS line ($\phi = 0$) and the OP line $\phi = \pi/2$ are shown in the upper and lower panel of Figure 3, respectively. The labels correspond to the vertical ordering of PEC for the four different impact parameter values ($b = 0.0$, 0.9, 1.8 and 3.6 a.u.) and the initial (dashed line) and final (full line) collision channels. As the impact parameter increases, the energy difference diminishes, converging to the asymptotic energy gain

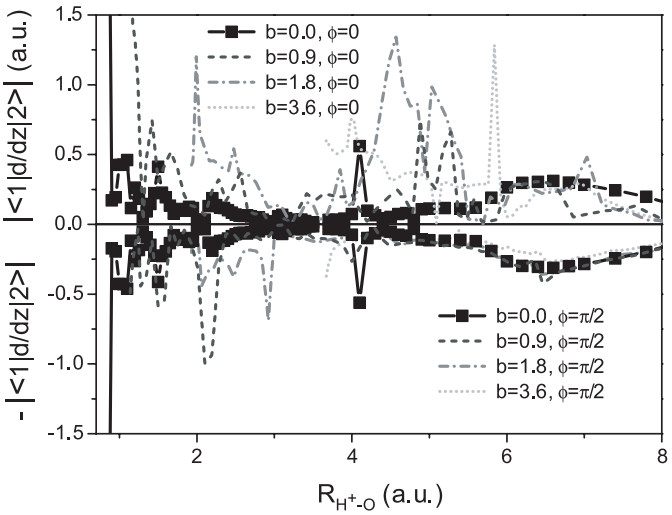

Fig. 4. Magnitude of the nonadiabatic coupling between the two states in Figure 1 ($\phi = 0$; positive sign) and Figure 2 ($\phi = \pi/2$, negative sign). Four impact parameters are considered in each case.

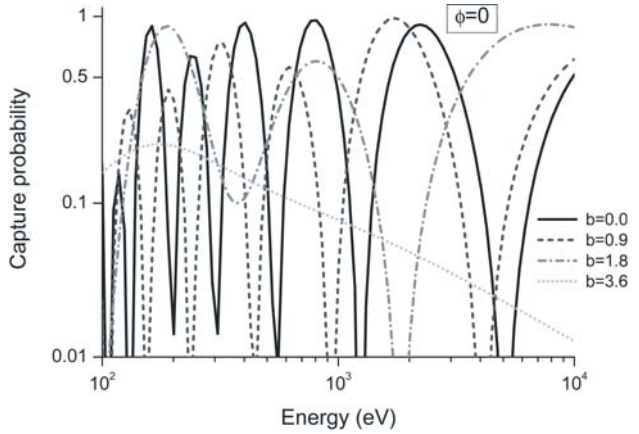

Fig. 5. Probability of electron capture along the four trajectories with $\phi = 0$.

value $E(H_2O) - E(H_2O^+) + 0.5$, which is approximately 0.0467 a.u. The absolute values of the non-adiabatic coupling between the initial and final state is shown in Figure 4 for all values of impact parameters and $\phi = 0$, $\pi/2$.

Solving the coupled equations (1) along the H^+ beam, we obtained the electron capture probability for each straight line trajectory. These are plotted e.g. in Figures 5 and 6, respectively, demonstrating a *marked* steric effect along each trajectory (curves labeled with $b = 0.0$, 0.9, 1.8 and 3.6). Except for $b = 0$, the angle between $\boldsymbol{R}_{O-H^+}$ (connecting the oxygen atom and the impacting proton) and the plane of water molecule varies in the full range from $-\pi/2$ through 0 to $\pi/2$, scanning the potential energy surface in a complex way. The probabilities of electron capture for $\phi = 0$ and $\phi = \pi/2$ exhibit oscillations as a function of energy, the frequency of which diminishes when b increases. Although for any fixed value of energy the capture probability substantially differs between $\phi = 0$ and $\phi = \pi/2$, the overall behavior (frequency of

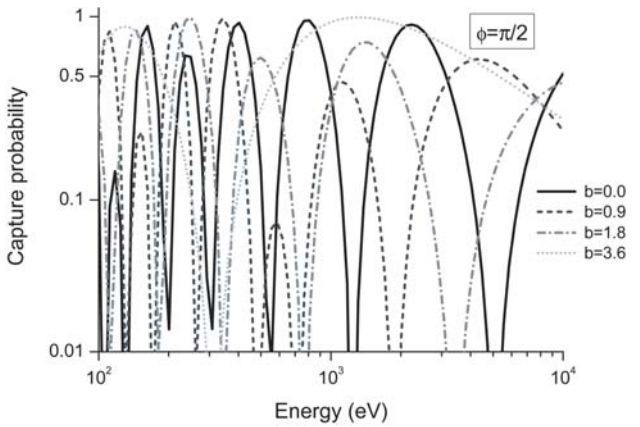

Fig. 6. Probability of electron capture along the four trajectories with $\phi = \pi/2$.

oscillations, relative heights of the peaks) is similar, except for the highest value of the impact parameter considered here, $b = 3.6$. This similarity between the two cases could be modeled analytically as Stueckelberg oscillations, e.g. in the 2-state exponential model [25], which is applicable since the asymptotic energy separation of electronic states is rather small and the coupling vanishes quite slowly both for $\phi = 0$ and $\phi = \pi/2$. In the two-state exponential model, the transition probability then behaves as $p \sim \sin^2(c_1/\sqrt{E} + c_2)$, where c_1 and c_2 are certain constants depending on the particular shape of the two potential energy curves and their asymptotic separation [25].

Finally, let us estimate the variation of the unresolved electron capture cross-section in the case of perpendicular collisions, based in equation (3). We can reasonably assess the variation of the cross-section integral (2) by altering the PEC projections Γ and studying the difference. This is formalized as follows.

Let us denote the fixed potential matrix as $\underline{V}(b_0, \phi_0, z)$. It is often the case that instead of the complete set of potential energy surfaces, here $\underline{V}(b, \phi, z)$ with $0 \leq b < R_t$ and $-\pi/2 < \phi < \pi/2$, only a few sets for fixed b_0 and ϕ_0 are available. In the following, we quantify the size of the error obtained by replacing $\underline{V}(b, \phi, z)$ with $\underline{V}(b_0, \phi_0, z)$.

Then we define the approximate cross-section value with the frozen potential energy surface, $\underline{V}(b, \phi, z) \sim \underline{V}(b_0, \phi_0, z)$, as

$$s_\perp(b_0, \phi_0) \equiv 2\pi \int_0^\infty \mathrm{d}b\, b\, p\left(b_0, \phi_0; R\left(\sqrt{b^2 + b_0^2}, z \to \infty\right)\right). \tag{4}$$

Note that by using various values of b_0 and ϕ_0 (ideally all points in the transition region), $s_\perp(b_0, \phi_0)$ (and $p_{n'}(b_0, \phi_0; R)$) can tell us how much the contributions to the physical cross-section in equation (3) vary across the space of b and ϕ, which closely relates to the accuracy of the approximate cross-section $s_\perp(b_0, \phi_0)$. It will be shown in the following that $s_\perp(b_0, \phi_0)$ is often a smooth and slowly varying function that can represent $\sigma_\perp$ accurately.

The most natural parameter choice is $b_0 = 0$ and $\phi_0 = 0$, in which case the quantity $s_\perp(0, 0)$ is hereafter

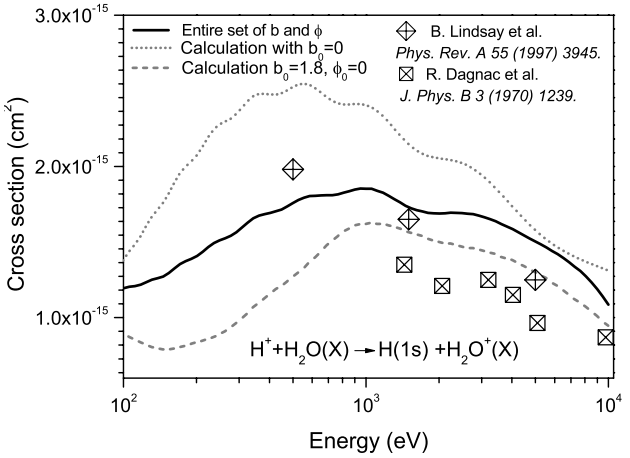

Fig. 7. Electron capture cross-section: experimental data and stereodynamical projections. The calculated curves correspond to an infinite beam of perpendicular trajectories ($0 \leq b < \infty$) using a frozen potential energy surface with parameters indicated in the figure; the spread between the curves is a useful accuracy measure of the central collision model.

referred to as the cross-section in the central collision approximation. In mathematical terms, the diabatic matrix $\underline{V}(b, \phi, z)$ is approximated by $\underline{V}(0, \cdot, z)$ for $0 \leq b < R_t$, where R_t is the size of the transition region. Physically, the boundary of the transition region is defined by requiring that for $R > R_t$ all coupling terms vanish. Then for $b > R_t$, the entire trajectory of the projectile remains outside of this transition region and no transitions can take place. The particular shape of the outside potential energy surfaces for $b > b_0$ thus plays no role in the physics of the scattering process. Therefore systems with more compact transition regions are more likely to be well approximated by using the potential energy surface for a central collision, $\underline{V}(0, 0, z)$.

Variation in the values of $s_\perp(b_0, \phi_0)$ (for b_0 falling in the transition region and arbitrary ϕ_0) then indicates the accuracy of the central collision approximation. We also note that the value $s_\perp(0, 0)$ corresponds to the fixed-γ approximation, which has been used extensively [26–28].

Both the full calculation with $\underline{V}(b_0, \phi_0, z)$ on the trajectories shown in Figure 1, and an approximate calculation with $b_0 = 0$ and $b_0 = 1.8$, $\phi_0 = 0$ were carried. The resulting cross-section $\sigma_\perp$ and the approximate values $s_\perp(0, 0)$ and $s_\perp(1.8, 0)$ are shown in Figure 7. Also the experimental values for single electron capture by proton on water molecule are shown in this Figure. The experimental cross-sections can be well reproduced by $s_\perp(0, 0)$ in accordance with our experience and previous work [4,26–28]. The difference between $s_\perp(0, 0)$, $s_\perp(1.8, 0)$, and the calculated cross-section $\sigma_\perp$ is found to be within the order of 50%.

Let us note that the experimental data for charge transfer cross-sections are typically reported with error bars of this or greater size [20–22], typically in graphical form with a logarithmic vertical scale; also discrepancies of an order of magnitude in the experimental data measured by different groups for the same process are not uncommon. Such discrepancies often arise from the presence of metastable ions in the projectile beam or various contamination of the beamline. Thus the results in Figure 7 tell us that the central collision approximation, $s_\perp(0, 0)$, is for instance a very reasonable tool to estimate the order and overall behavior of charge transfer cross-sections when designing new experiments, or when resolving the discrepancies sized by an order of magnitude in the measured data.

More interestingly, the size of the steric effect on the electron capture cross-section, which is bound by about 50%, is much smaller than the steric effect in transition probabilities (cf. the fast oscillations, their different frequencies, and the vertical logarithmic scale in Figs. 5 and 6). Therefore, at keV/amu energies, the steric effect can be seen along particular straight line trajectories, but averages out to large extent in the integral values of the cross-section. This interesting finding is demonstrated by the dramatic variance of transition probabilities in Figures 5 and 6 vs. the smooth behavior of the integral cross-section σ (or its approximate values $s(b_0, \phi_0)$) in Figure 7.

4 Concluding remarks

In this paper, we have first discussed the steric effect in the charge transfer collisions of the metastable $O^+(^2D)$ ion with H_2. The steric effect in the keV range of collision energies, defined as the cross-section ratio for the H_2 molecule aligned at a fixed angle toward the $O^+(^2D)$ beam, varies in the range of 30% of the orientation-unresolved cross-section, an effect which falls within the error bars of most electron capture experiments. We further observed a marked steric effect in the electron capture probabilities for individual rays in an H^+ beam oriented perpendicular to the plane of the H_2O target molecule.

The steric characteristics of charge transfer probabilities are pronounced in the entire energy range studied, i.e. 100 eV/amu to 10 keV/amu. This is in contrast to the common belief that steric effects should be small for high energies, an intuition based merely on the analysis of integral cross-sections. The opposite is true; in addition, the collision trajectories at keV/amu energies are straight lines, which provides a theoretically interesting method for probing the details of the potential energy surface in collisions. Experiments in this direction are highly desirable for a better understanding of the charge transfer phenomenon and comparison with theory.

We have also developed a criterion to assess the variation of the cross-section integral based on a sample of projectile trajectories from the beam, or the details of the potential energy surface. Using this criterion, the calculated cross-section, and the experimental data available, it was demonstrated that the central collision approximation yields a very reasonable value of the capture cross-section, which is useful in estimating the order of cross-section magnitude for design of new experiments or even resolving large discrepancies in cross-section measurements by various experimental groups.

This work was supported in part by the Japan Society for the Promotion of Science (JSPS), the Japanese Ministry of Science, Sports, Culture and Education (MEXT), and by the grant BU 450/7-3 of the Deutsche Forschungsgemeinschaft and the Fonds der Chemischen Industrie. L. Pichl acknowledges support by a JSPS Grant-in-Aid, Max Planck Society, and the Academic Frontier Program by MEXT. Special thanks are due to Prof. T. Kasai.

References

1. M. Kimura, N.F. Lane, Adv. At. Mol. Opt. Phys. **26**, 79 (1989)
2. V. Sidis, Adv. At. Mol. Phys. **26**, 161 (1989)
3. L. Pichl, Y. Li, H.-P. Liebermann, R.J. Buenker, M. Kimura, J. Chem. Phys. **118**, 4872 (2003)
4. L. Pichl, Y. Li, H.-P. Liebermann, R.J. Buenker, M. Kimura, Phys. Rev. A **69**, 062715 (2004)
5. R.J. Buenker, S.D. Peyerimhoff, Theo. Chim. Acta **35**, 33 (1974); R.J. Buenker, S.D. Peyerimhoff, Theo. Chim. Acta **39**, 217 (1975); R.J. Buenker, Int. J. Quant. Chem. **29**, 435 (1986)
6. R.J. Buenker, in *Proceedings of the Workshop on Quantum Chemistry and Molecular Physics*, Wollongong, Australia, edited by P.G. Burton (Wollongong University Press, Wollongong, Australia, 1980); in *Studies in Physical and Theoretical Chemistry*, edited by R. Carbo (Elsevier, Amsterdam, 1981), Vol. 21, p. 17; R.J. Buenker, R.A. Phillips, J. Mol. Struc.: Theochem **123**, 291 (1985)
7. S. Krebs, R.J. Buenker, J. Chem. Phys. **103**, 5613 (1995)
8. G. Hirsch, P.J. Bruna, R.J. Buenker, S.D. Peyerimhoff, Chem. Phys. **45**, 335 (1980)
9. T.H. Dunning Jr, J. Chem. Phys. **90**, 1007 (1989)
10. M. Kimura, Y. Li, G. Hirsch, R.J. Buenker, Phys. Rev. A **52**, 1196 (1995); M. Kimura, Y. Li, G. Hirsch, R.J. Buenker, Phys. Rev. A **54**, 5019 (1996)
11. R.J. Buenker, D.B. Knowles, S.N. Rai, G. Hirsch, K. Bhanuprakash, J.R. Alvarez-Collado, in: *Quantum Chemistry - Basic Aspects, Actual Trends*, Studies in Physical and Theoretical Chemistry), edited by R. Carbo (Elsevier, Amsterdam, 1989), Vol. 62, p. 181
12. D.B. Knowles, J.R. Alvarez-Collado, G. Hirsch, R.J. Buenker, J. Chem. Phys. **92**, 585 (1990)
13. T.G. Winter, N.F. Lane, Phys. Rev. A **17**, 66 (1978)
14. M. Kimura, A.B. Sannigrahi, J.P. Gu, G. Hirsch, R.J. Buenker, I. Shimamura, Astrophys. J. **473**, 1114 (1996)
15. J.B. Delos, Rev. Mod. Phys. **53**, 287 (1981)
16. W. Fritsch, C.D. Lin, Phys. Rev. A **54**, 4931 (1996)
17. J.G. Wang, P.C. Stancil, A.R. Turner, D.L. Cooper, Phys. Rev. A **69**, 062702 (2004)
18. L.F. Errea, L. Fernandez, A. Macias, L. Mendez, I. Rabadan, A. Riera, Phys. Rev. A **69**, 012705 (2004)
19. L.F. Errea, A. Macias, L. Mendez, B. Pons, A. Riera, J. Chem. Phys. **119**, 325 (2003)
20. X. Li, Y.-L. Huang, G.D. Flesch, C.Y. Ng, J. Chem. Phys. **106**, 564 (1997)
21. W.L. Nutt, R.W. McCullough, H.B. Gilbody, J. Phys. B: At. Mol. Phys. **12**, L157 (1979)
22. R.A. Phaneuf, F.W. Meyer, R.H. McKnight, Phys. Rev. A **17**, 534 (1978)
23. T. Kusakabe et al., Phys. Rev. A **60**, 344 (1999)
24. T. Kusakabe et al., J. Phys. B: At. Mol. Opt. Phys. **34**, 4809 (2001)
25. E.E. Nikitin, S.Ya. Umanskii, *Theory of Slow Atomic Collisions* (Springer, New York, 1984)
26. R. Suzuki, S.N. Rai, H.-P. Liebermann, R.J. Buenker, L. Pichl, M. Kimura, Phys. Rev. A **71**, 032710 (2005)
27. H. Suno, S.N. Rai, H.-P. Liebermann, R.J. Buenker, M. Kimura, R.K. Janev, Phys. Rev. A **70**, 032703 (2004)
28. T. Kusakabe, K. Asahina, J.P. Gu, G. Hirsch, R.J. Buenker, M. Kimura, H. Tawara, Y. Nakai, Phys. Rev. A **62**, 062714 (2000)